

Relative Occurrence Rate Between Hot and Cold Jupiters as an Indicator to Probe Planet Migration

TIANJUN GAN ¹, KANGROU GUO ², BEIBEI LIU ^{3,4}, SHARON X. WANG ¹, SHUDE MAO ¹,
JOHANNES BUCHNER ⁵ AND BENJAMIN J. FULTON ^{6,7}

¹*Department of Astronomy, Tsinghua University, Beijing 100084, People's Republic of China*

²*Tsung-Dao Lee Institute, Shanghai Jiao Tong University, 520 Shengrong Road, Shanghai 201210, People's Republic of China*

³*Institute for Astronomy, School of Physics, Zhejiang University, Hangzhou 310027, People's Republic of China*

⁴*Center for Cosmology and Computational Astrophysics, Institute for Advanced Study in Physics, Zhejiang University, Hangzhou 310027, People's Republic of China*

⁵*Max-Planck-Institut für extraterrestrische Physik, Giessenbachstrasse 1, D-85748 Garching, Germany*

⁶*Cahill Center for Astronomy & Astrophysics, California Institute of Technology, Pasadena, CA 91125, USA*

⁷*IPAC-NASA Exoplanet Science Institute, Pasadena, CA 91125, USA*

ABSTRACT

We propose a second-order statistic parameter ε , the relative occurrence rate between hot and cold Jupiters ($\varepsilon = \eta_{\text{HJ}}/\eta_{\text{CJ}}$), to probe the migration of gas giants. Since the planet occurrence rate is the combined outcome of the formation and migration processes, a joint analysis of hot and cold Jupiter frequency may shed light on the dynamical evolution of giant planet systems. We first investigate the behavior of ε as the stellar mass changes observationally. Based on the occurrence rate measurements of hot Jupiters (η_{HJ}) from the TESS survey and cold Jupiters (η_{CJ}) from the CLS survey, we find a tentative trend (97% confidence) that ε drops when the stellar mass rises from 0.8 to 1.4 M_{\odot} , which can be explained by different giant planet growth and disk migration timescales around different stars. We carry out planetesimal and pebble accretion simulations, both of which could reproduce the results of η_{HJ} , η_{CJ} and ε . Our findings indicate that the classical core accretion + disk migration model can explain the observed decreasing trend of ε . We propose two ways to increase the significance of the trend and verify the anti-correlation. Future works are required to better constrain ε , especially for M dwarfs and for more massive stars.

Keywords: Giant Planets, Occurrence Rate, Planet Formation and Migration

1. INTRODUCTION

About three decades after the first discovery of a hot Jupiter around a Solar-type star (Mayor & Queloz 1995), the predominant mechanism of their formation remains unclear. Three leading hypotheses have been proposed including in-situ formation, disk as well as tidal migration (Dawson & Johnson 2018). Thanks to a series of successful ground (e.g, Bakos et al. 2004; Pollacco et al. 2006; Pepper et al. 2007; Chazelas et al. 2012) and space (e.g., Baglin et al. 2006; Borucki et al. 2010; Howell et al. 2014; Ricker et al. 2015) surveys, the increasing sample of giant planets enables numerous subsequent statistical

studies, which in turn offer unprecedented opportunities to testify these scenarios.

One of the key demographic parameters is the occurrence rate. Based on the observations from the *Kepler* mission (Borucki et al. 2010), it has been demonstrated that about 0.5% Sun-like stars host a hot Jupiter with orbital period shorter than 10 days (Fressin et al. 2013; Petigura et al. 2018; Howard et al. 2012), consistent with the results from early ground-based transit surveys (Gould et al. 2006; Kovács et al. 2013). Despite that radial velocity surveys infer a larger hot Jupiter occurrence rate by a factor of two (Endl et al. 2006; Cumming et al. 2008; Mayor et al. 2011), such difference might be due to different stellar sample properties like metallicity and binary fraction (Wright et al. 2012; Moe & Kratter 2021; Chen et al. 2023). In contrast, cold Jupiters are more common with an occurrence rate about 5 – 15% (Johnson et al. 2010; Wittenmyer et al. 2020; Fulton et al.

2021; Sabotta et al. 2021), which is predicted by both the core accretion (Pollack et al. 1996; Liu & Ji 2020) and the gravitational instability (Boss 1997) planet formation theory.

Plenty of efforts have been made so far to study the giant planet occurrence rate as a function of stellar type. By splitting the full mixed stellar sample into different mass bins, both Zhou et al. (2019) and Beleznyay & Kunimoto (2022) claimed a possible anti-correlation between the hot Jupiter occurrence rate and host mass. *Kepler* was designed to measure the occurrence rates of different planet systems, which yields good constraint on small planets around M dwarfs (Dressing & Charbonneau 2013, 2015; Morton & Swift 2014; Muirhead et al. 2015; Mulders et al. 2015; Gaidos et al. 2016; Hardegree-Ullman et al. 2019; Bryson 2020). However, it has not been able to provide a similar measurement on giant planets due to the limited number of monitored M dwarfs (Johnson et al. 2012). With the help of the Transiting Exoplanet Survey Satellite (*TESS*; Ricker et al. 2015), Gan et al. (2023) and Bryant et al. (2023) recently extended the occurrence rate function to M dwarfs, where they found that it falls from G dwarfs to the low-stellar-mass end. Meanwhile, the occurrence of cold Jupiters seems to enhance with increasing host mass (Johnson et al. 2010; Fulton et al. 2021). Statistical work from Wolthoff et al. (2022) pointed out that the fraction likely peaks around stars with a mass around $1.7 M_{\odot}$ and then drops towards stars of $4 M_{\odot}$ (see also Reffert et al. 2015), consistent with the conclusion from the population synthesis study carried out by Johnston et al. (2023). Such a stellar mass-dependent feature of giant planet occurrence rate is expected to be an outcome of different amounts of total dust materials. Generally, there are more abundant solids in the protoplanetary disk of high mass stars (e.g., Andrews et al. 2013), favoring giant planet formation. Nevertheless, the short disk lifetime of A stars compared with Sun-like stars (Ribas et al. 2015) and planet engulfment (Stephan et al. 2018) may lead to a low rate of survived giant planets, which probably explains the parabola-shaped giant planet occurrence rate.

Although the giant planet occurrence rate is supposed to be an intrinsic characteristic, which is bound up with their formation history, later inward migration presumably also leaves some signatures (Lin et al. 1996; Burkert & Ida 2007). Since stellar mass plays a role in both formation and migration, investigating the occurrence rate of hot and cold Jupiters separately is probably insufficient to untangle the impact from each process. A joint analysis of these occurrence measurements around stars

with different masses may provide clues on the dynamical evolution of giant planets.

To date, various planet formation simulation codes have been developed to investigate the behaviours of planets at the early stage of their formation (Ida & Lin 2004; Mordasini et al. 2009; Liu et al. 2019; Schoonenberg et al. 2019; Guo & Kokubo 2021; Burn et al. 2021; Pan et al. 2024), which also allow for tracking their migration, enabling us to look into how two processes affect giant planet occurrence rate simultaneously. In this paper, we explore the behavior of relative occurrence rate between hot and cold Jupiters at different stellar mass based on statistics from large surveys. We then carry out planetesimal and pebble-driven simulations to examine whether the standard core accretion + disk migration model can reproduce the observation result. A similar study was also carried out by Su et al. (2024) who investigate the mutual occurrence ratio of giant planets based on RV surveys but using different definitions on hot and cold Jupiters. The paper is organized as follows. In Section 2, we describe how we construct and combine the observation sample. Section 3 presents the details of our simulations. We discuss and conclude our findings in Section 4.

2. OBSERVATION RESULTS

In order to make a reliable comparison between observations and simulations, we follow the definition below throughout the paper. We define hot Jupiters (HJs) as planets with mass $100 M_{\oplus} \leq M_p \leq 13.6 M_J$ and semi-major axis $0.02 \leq a \leq 0.1$ au while cold Jupiters (CJs) as companions with the same mass cut but locating at $1 \leq a \leq 5$ au. Since we attempt to compare the giant planet occurrence rate η , the number of planets N_p per 100 stars, across different semi-major axis and stellar mass, we make use of demographic results from the same technique and homogeneous survey for each (HJs and CJs) sample to minimize possible observation bias.

2.1. Occurrence Rate of HJs

The results of HJ occurrence rate (η_{HJ}) around different stars are taken from statistical works based on the *TESS* survey (Ricker et al. 2015). We use the occurrence rates of HJs with $0.8 \leq R_p \leq 2.5 R_J$ and $0.9 \leq P_b \leq 10$ days around AFG stars obtained by Beleznyay & Kunimoto (2022): $0.29 \pm 0.05\%$ for A stars ($1.4\text{--}2.3 M_{\odot}$), $0.36 \pm 0.06\%$ for F stars ($1.05\text{--}1.4 M_{\odot}$), and $0.55 \pm 0.14\%$ for G stars ($0.8\text{--}1.05 M_{\odot}$). Regarding HJs ($0.6 R_J \leq R_p \leq 2.0 R_J$ and $1 \leq P_b \leq 10$ days) around M dwarfs, we use the frequency reported by Bryant et al. (2023). The authors divided the full M dwarf sample into sub groups and measured individual

η_{HJ} of $0.137 \pm 0.097\%$ ($0.088\text{--}0.26 M_{\odot}$), $0.108 \pm 0.083\%$ ($0.26\text{--}0.42 M_{\odot}$), and $0.29 \pm 0.15\%$ ($0.42\text{--}0.71 M_{\odot}$). Table 1 lists the summary of these results. We emphasize that the HJs are defined in the orbital period and planet radius dimensions among transit surveys, which are different from our definition above based on semi-major axis and planet mass. Therefore, we examine the effect that may be induced by such differences.

Under the definition of Beleznyay & Kunimoto (2022), the semi-major axis ranges of HJs are [0.022, 0.111], [0.019, 0.097] and [0.018, 0.088] au around A, F and G stars, respectively. All of them are roughly consistent with our boundary cut [0.02, 0.1] au within about 0.01 au, hence we neglect the difference here. Meanwhile, according to the planet period and stellar mass cut in Bryant et al. (2023), the semi-major axis ranges of HJs around M stars especially mid-to-late M dwarfs are smaller: [0.011, 0.051], [0.014, 0.063] and [0.016, 0.075] au for the $0.088 - 0.26 M_{\odot}$, $0.26 - 0.42 M_{\odot}$ and $0.42 - 0.71 M_{\odot}$ mass bin. We thus only focus on the η_{HJ} around early-M dwarfs with the semi-major axis range closest to our definition for consistency.

More importantly, we have to be sure the radii range ([0.8, 2.5] R_J) defined for the transit occurrence estimates would be consistent with the mass range ([100 M_{\oplus} , 13.6 M_J]) defined for Jupiters in this work. Note that the radius boundary of HJs adopted in Beleznyay & Kunimoto (2022) and Bryant et al. (2023) is different ([0.8, 2.5] and [0.6, 2.0] R_J). Since no inflated giant planets around M dwarfs with radius above 2.0 R_J have been found yet and the completeness in the statistics will not change significantly given the large transit depth, corresponding to a high signal-to-noise ratio in transit signal search, we thus consider the change of upper boundary from 2.0 to 2.5 R_J will not affect the final occurrence rate estimate.

However, the difference in the lower radius boundary is expected to have an effect. Among 15 planet candidates included in Bryant et al. (2023), a total of three objects have radius between 0.6 and 0.8 R_J , one of which orbits an early-M dwarf. To correct the radius effect, we compute the occurrence rate of HJs with radius between 0.8 and 2.5 R_J around early-M dwarfs based on the completeness map¹ provided in Bryant et al. (2023) following the same procedure therein, and we derive an occurrence rate of $0.23 \pm 0.15\%$. This calibrated result is close to the original value $0.29 \pm 0.15\%$ reported in Bryant et al. (2023).

¹ We use the map with radius between 0.8 and 2.0 R_J to estimate the average completeness.

Next, we retrieve a list of hot Jupiters with precise mass measurements around AFG and M dwarfs with $0.8 \leq R_p \leq 2.5 R_J$ and $1.0 \leq P_b \leq 10$ days from NASA Exoplanet Archive (Akeson et al. 2013). We find that we will exclude about 7.2% and 6.7% HJs around AFG and M dwarfs if using our planet mass cut $\geq 100 M_{\oplus}$ instead to define HJs. This difference cannot be corrected statistically unless we have mass measurements for all planet candidates included in both Beleznyay & Kunimoto (2022) and Bryant et al. (2023), which are not available and beyond the scope of this study. Consequently, we regard it as a 10% uncertainty in η_{HJ} , a small change in the occurrence rate but well within the error bar, when interpreting our results.

Through the above tests, we consider that both the semi-major axis range and the change from radius to mass cut have little impact on η_{HJ} , which will not affect our final conclusion. We take all η_{HJ} around AFG from Beleznyay & Kunimoto (2022) and the recalculated η_{HJ} measurement around early-M dwarfs based on Bryant et al. (2023) into account in the analysis below.

2.2. Occurrence Rate of CJs

The CJ occurrence rate (η_{CJ}) around stars with different mass are taken from Fulton et al. (2021) delivered by the California Legacy Survey (CLS; Rosenthal et al. 2021). Through the radial velocity measurements for a selected sample of FGKM stars collected under the CLS program, Fulton et al. (2021) determined the occurrence of giant planets beyond the ice line. To be specific, the authors measured the frequency of cold Jupiters ($100 \leq M_p \leq 6000 M_{\oplus}$) within 1–5 au around stars with different mass.

Although the semi-major axis range is the same, the mass upper boundary (6000 M_{\oplus}) in Fulton et al. (2021) is higher than our threshold (13.6 M_J). However, among the total 177 objects, only one sub-stellar companion HD 168443c locates within the semi-major axis limit 1–5 au that we pay attention to. HD 168443c has a mass of $17.76 \pm 0.35 M_J$ and a semi-major axis of 2.88 ± 0.03 au orbiting a Sun-like star (Rosenthal et al. 2021). Since the difference on η_{CJ} after excluding this single object from the total sample is within the 1σ uncertainty, we consider that it has a negligible effect on our study. Table 1 summarizes the giant planet occurrence rate results used in this work.

Given the large uncertainty of η_{CJ} on M dwarfs due to the very small sample size, we also investigate results from other studies. Johnson et al. (2010) measured a rate about $3.4^{+2.2}_{-0.9}\%$ of M stars with mass below $0.6 M_{\odot}$ hosting a gas giant with $M_p > 0.3 M_J$ within 2.5 AU. Montet et al. (2014) determined that about $6.5 \pm 3.5\%$

M dwarfs ($0.10 - 0.64 M_{\odot}$) host giant planets within 20 AU with mass $1 \leq M_p \leq 13 M_J$. Based on the CARMENES RV blind survey, Sabotta et al. (2021) found an occurrence rate upper limit of 7% for giant planets ($100 - 1000 M_{\oplus}$) around M dwarfs with period between 100 and 1000 days. Since the definitions of CJs in these studies and the M dwarf mass ranges are fairly different from this work, we choose not to include these measurements.

2.3. Observed Relative Occurrence Rate Between HJs and CJs

After two samples are constructed, we investigate the dependence of relative occurrence rate on stellar mass. The relative occurrence rate is defined as the fraction between HJs and CJs ($\varepsilon = \eta_{\text{HJ}}/\eta_{\text{CJ}}$), which depicts the number ratio (or probability ratio) of giant planets $N_{p,\text{HJ}}/N_{p,\text{CJ}}$ within two different semi-major axis ranges around a star. If HJs originally form beyond the snow line and migrate inward, then ε quantifies the efficiency of such process. A single measurement of ε in a certain stellar mass bin is less meaningful if the span of two semi-major axis ranges are different (i.e., without normalizing to the same semi-major axis level dN/da). Nevertheless, through investigating the evolution of ε with stellar mass, we are able to glimpse into the efficiency of planet formation and migration processes around different types of stars. In principle, the relative giant planet occurrence rate is determined by the planet formation and migration history, both of which will affect the frequency of giant planets at different distance from the hosts.

We first calibrate the occurrence rates of HJs, making the comparison with the occurrence rates CJs is performed in the same stellar mass bins. Assuming each η_{HJ} measurement from real observations has a normal distribution, we randomly generate 50,000 sets of η_{HJ} of four mass ranges used in Beleznyay & Kunimoto (2022) and Bryant et al. (2023), centering at 0.565, 0.925, 1.225 and $1.850 M_{\odot}$ ². We then linearly interpolate these outputs to five stellar mass bin 0.6, 0.8, 1.0, 1.2 and $1.4 M_{\odot}$ adopted by Fulton et al. (2021), which are the central values with a bin size of $0.2 M_{\odot}$. Figure 1 illustrates the η_{HJ} distribution of our interpolations. We adopt the median value and standard deviation of each distribution as the occurrence rate and uncertainty used for further analysis. Finally, we compute the ε of each stellar mass bin by dividing the η_{HJ} and η_{CJ} , where the uncertainty

is determined through error propagation. We list η_{HJ} , η_{CJ} and the derived ε in Table 2.

Figure 2 shows the individual occurrence rate η and the relative occurrence ε as a function of stellar mass. Although only limited measurements are available and the ε of M stars is poorly constrained due to the large uncertainty of η_{CJ} , we spot a possible downward trend of ε with increasing stellar mass (see the right panel of Figure 2), consistent with the findings reported in Su et al. (2024). We next examine the significance of the decreasing trend through two ways. Since the result on M dwarfs is highly uncertain, we exclude this data point during our analysis. First, we measure the Pearson’s r correlation coefficient between the other four ε measurements and stellar mass, where we find a weak anti-correlation ($r = -0.88$) with a p-value of 0.12. We also carry out Monte Carlo simulations based on the derived ε values listed in Table 2. Since the final results of ε have asymmetrical lower $\sigma_{\varepsilon,\text{lerr}}$ and upper $\sigma_{\varepsilon,\text{uerr}}$ uncertainties, we randomly draw data sets of ε of each stellar mass bin from two half-normal distributions, and select physically meaningful positive η values. We fit a linear function between ε and stellar mass: $\varepsilon = k \cdot (M_{\star}/M_{\odot}) + b$. The best-fits are found through the least square method using `scipy.optimize`. We repeat the same step for 10,000 times and record the best-fit slope k and intercept b of each simulated data set. We find that 96.7% of all fitted curves are descending with stellar mass. We also sample from skewed normal distributions using `scipy.stats.skewnorm` with 1 sigma quantiles matching the observational error bars for each stellar mass bin, and fit linear functions between ε and stellar mass. We find similar results that 97.1% of simulated data sets have negative slopes. For a Gaussian probability distribution, this probability, considering both tails, corresponds to a 2.2σ confidence level. We show the distribution of best-fit slopes we obtained in Figure 3, where the best-fit relation is

$$\varepsilon = \frac{\eta_{\text{HJ}}}{\eta_{\text{CJ}}} = [-0.08 \pm 0.04] \cdot \left(\frac{M_{\star}}{M_{\odot}} \right) + [0.12 \pm 0.05]. \quad (1)$$

At this point, we can only report a tentative anti-correlation trend between ε and stellar mass. We provide two ways to increase the significance of the signal in Section 4.3.

If such a trend indeed exists and is confirmed by future observations, it might be owing to the dependence of the growth as well as migration timescale of giant planets on the stellar mass, which allows testing the dominant roles of theoretical models and hypotheses. Therefore, it motivates the simulations we carried out in Section 3.

² These are the central values of each stellar mass bin (See Table 1).

Table 1. Summary of literature giant planet occurrence rates used in this work.

Hot Jupiters ^[1]						
Stellar mass range (M_\odot)	0.088 – 0.26	0.26 – 0.42	0.42 – 0.71	0.8 – 1.05	1.05 – 1.4	1.4 – 2.3
η_{HJ} (%)	0.14 ± 0.10	0.11 ± 0.08	0.29 ± 0.15	0.55 ± 0.14	0.36 ± 0.06	0.29 ± 0.05
Semi-major axis range (AU) ^[2]	0.011 – 0.051	0.014 – 0.063	0.016 – 0.075	0.018 – 0.088	0.019 – 0.097	0.022 – 0.111
Cold Jupiters ^[3]						
Stellar mass range (M_\odot)	0.5 – 0.7	0.7 – 0.9	0.9 – 1.1	1.1 – 1.3	1.3 – 1.5	
η_{CJ} (%)	$0.50^{+2.93}_{-0.50}$	$6.26^{+2.57}_{-1.40}$	$16.04^{+3.69}_{-2.34}$	$18.78^{+5.81}_{-4.28}$	$16.95^{+17.24}_{-3.82}$	
Semi-major axis range (AU)	1 – 5	1 – 5	1 – 5	1 – 5	1 – 5	

[1] Results taken from [Beleznyay & Kunimoto \(2022\)](#) and [Bryant et al. \(2023\)](#).

[2] The boundary of semi-major axis is computed based on the stellar mass and planet orbital period range explored in two works.

[3] Results taken from [Fulton et al. \(2021\)](#).

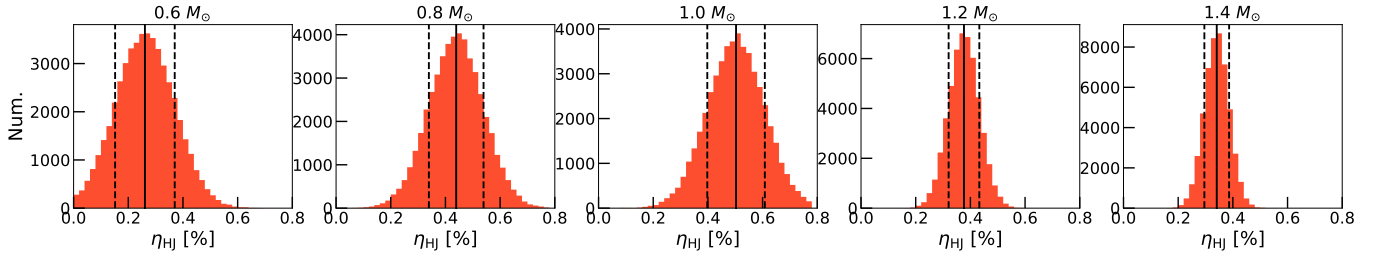


Figure 1. The η_{HJ} distribution of interpolation results from 50,000 randomly generated data sets (see Section 2.3 for details). Different panels represent results of different stellar masses. The median and standard deviation of each distribution are shown as the black solid and dashed lines, and listed in Table 2.

Table 2. Final individual and relation occurrence rates used in this work.

Stellar mass bin (M_\odot) ^[1]	0.6	0.8	1.0	1.2	1.4
$\eta_{\text{HJ}}^{[2]}$ (%)	0.261 ± 0.109	0.439 ± 0.099	0.503 ± 0.105	0.376 ± 0.056	0.341 ± 0.045
$\eta_{\text{CJ}}^{[3]}$ (%)	$0.50^{+2.93}_{-0.50}$	$6.26^{+2.57}_{-1.40}$	$16.04^{+3.69}_{-2.34}$	$18.78^{+5.81}_{-4.28}$	$16.95^{+17.24}_{-3.82}$
$\varepsilon = \eta_{\text{HJ}}/\eta_{\text{CJ}}$	$0.522^{+0.565}_{-0.522}$ ^[4]	$0.070^{+0.022}_{-0.032}$	$0.031^{+0.008}_{-0.010}$	$0.020^{+0.005}_{-0.007}$	$0.020^{+0.005}_{-0.020}$

[1] These are the central value with a bin size of $0.2 M_\odot$.

[2] All η_{HJ} here are the median value from the interpolation results shown in Figure 1.

[3] Same as the results listed in Table 1, taken from [Fulton et al. \(2021\)](#).

[4] We exclude this point during our analysis since it is poorly constrained due to the large uncertainty of η_{CJ} on M dwarfs reported in [Fulton et al. \(2021\)](#).

3.1. Timescale Analysis

We first provide an analytical estimates on how the growth and disk migration of the planets depend on stellar mass. These two timescales can be expressed as

$$\tau_{\text{mig}} = f_{\text{mig}}^{-1} \left(\frac{M_\star}{M_{\text{p}}} \right) \left(\frac{M_\star}{\Sigma_{\text{g}} r^2} \right) h_{\text{g}}^2 \Omega_{\text{K}}^{-1} \propto M_\star^{3/4}, \quad (2)$$

$$\tau_{\text{grow}} = \frac{M_{\text{p}}}{M_{\text{PA}}} = \frac{M_{\text{p}}}{M_{\text{peb}} \epsilon_{\text{PA}}} \propto M_\star^{2/3-\beta}, \quad (3)$$

where f_{mig} is the migration prefactor, h_{g} is the disk aspect ratio, Ω_{K} is the Keplerian angular velocity, Σ_{g} is the gas density, r is the radial distance, \dot{M}_{g} , \dot{M}_{peb} are the gas flux and pebble flux ($\dot{M}_{\text{peb}} \propto \dot{M}_{\text{g}} \propto M_\star^\beta$ is assumed), and ϵ_{PA} is the pebble accretion efficiency ($\epsilon_{\text{PA}} \propto (M_{\text{p}}/M_\star)^{2/3}$) in the 2D shear regime ([Liu & Ormel 2018](#)). In the latter part of the above derivations we only consider the stellar mass scaling and adopt Σ_{g} and h_{g} from the inner

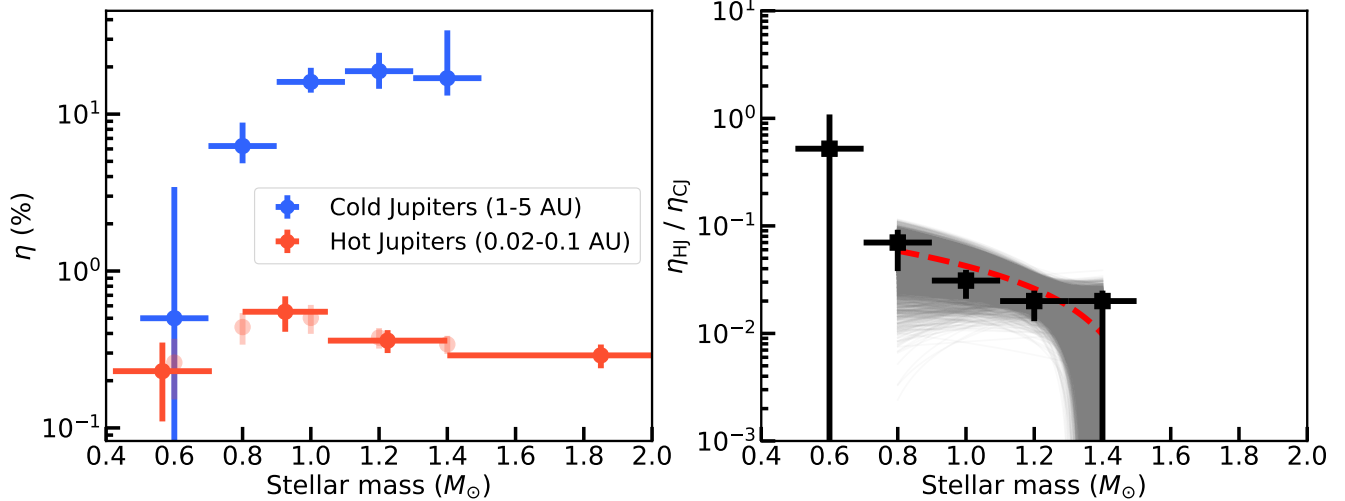


Figure 2. *Left Panel:* Observed occurrence rate of hot Jupiters (η_{HJ}) and cold Jupiters (η_{CJ}) as a function of stellar mass. The results of HJs (red) and CJs (blue) are taken from the *TESS* transit survey (Beleznyay & Kunimoto 2022; Bryant et al. 2023) and CLS RV survey (Fulton et al. 2021). Five translucent red dots are the median value of 50,000-time interpolation results (see Section 2.3). *Right Panel:* Relative occurrence rate ε between HJs and CJs ($\varepsilon = \eta_{\text{HJ}}/\eta_{\text{CJ}}$) vs. stellar mass. The gray lines mark the best-fit 1d polynomial functions between ε and M_\star of 10,000 randomly generated data sets while the red dashed line represents the median result. The horizontal uncertainties in both panels mark the stellar mass range. A possible decreasing trend of ε with increasing stellar mass can be seen.

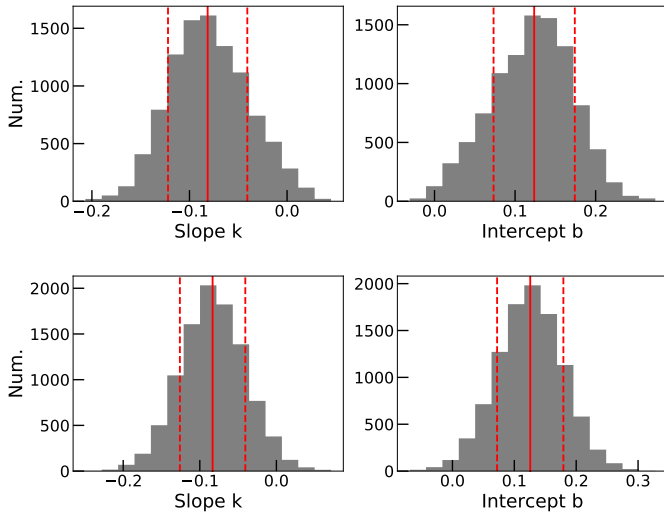


Figure 3. The slope and intercept distributions of the linear function fits to 10,000 sets of randomly generated ε based on observations shown in Figure 2. The top panel shows the results from simulations based on two half normal distributions while the bottom panel is the outputs from a continuous skewed normal distribution (see Section 2.3 for details). The red solid and dashed lines represent the median and standard deviation of the distributions. About 97% data sets have decreasing trends between relative occurrence rate ε and stellar mass M_\star .

viscous heating disk region of Liu et al. (2019). Observations indicate that $\beta \approx 1-1.8$ (Hartmann et al. 2016). As such, we can see from Eqs. 2 and 3 that the migration

timescale increases with M_\star while the growth timescale decreases with M_\star . In other words, planets grow faster with slow migration speed as their stellar host mass increases³. This consequently results in a decreasing trend of ε with M_\star .

To further test the above hypothesis, we run planetesimal and pebble accretion population synthesis simulations, examining whether the observed correlation can be reproduced numerically under the core accretion and disk migration framework. In general, the planetesimal accretion model assumes that protoplanets grow by pairwise collisions and accumulation of km-size planetesimals, while the pebble accretion model assumes that protoplanets grow by accreting mm- to cm-size pebbles. The key difference lies in the role that gas drag plays during the accretion process (Drażkowska et al. 2023). In order to make a comparison with observations, for both models we use the same definition of HJ and CJ as stated in Section 2, and consider the stellar mass range of 0.6 to 1.4 M_\odot , in which both η_{HJ} and η_{CJ} data are available. We describe the model setups below.

3.2. Planetesimal and Pebble Accretion Simulation

³ Although this derivation is based on pebble accretion, this anti-correlated $M_\star - \tau_{\text{grow}}$ scaling also applies to planetesimal accretion (see Eq.10 of Liu & Ji 2020). Besides, gas accretion does not alter this M_\star scaling. This is due to the Kelvin-Helmholtz contraction following a runaway fashion, which relies on the planet's mass and envelope opacity, without involving any M_\star dependence (Ikoma et al. 2000).

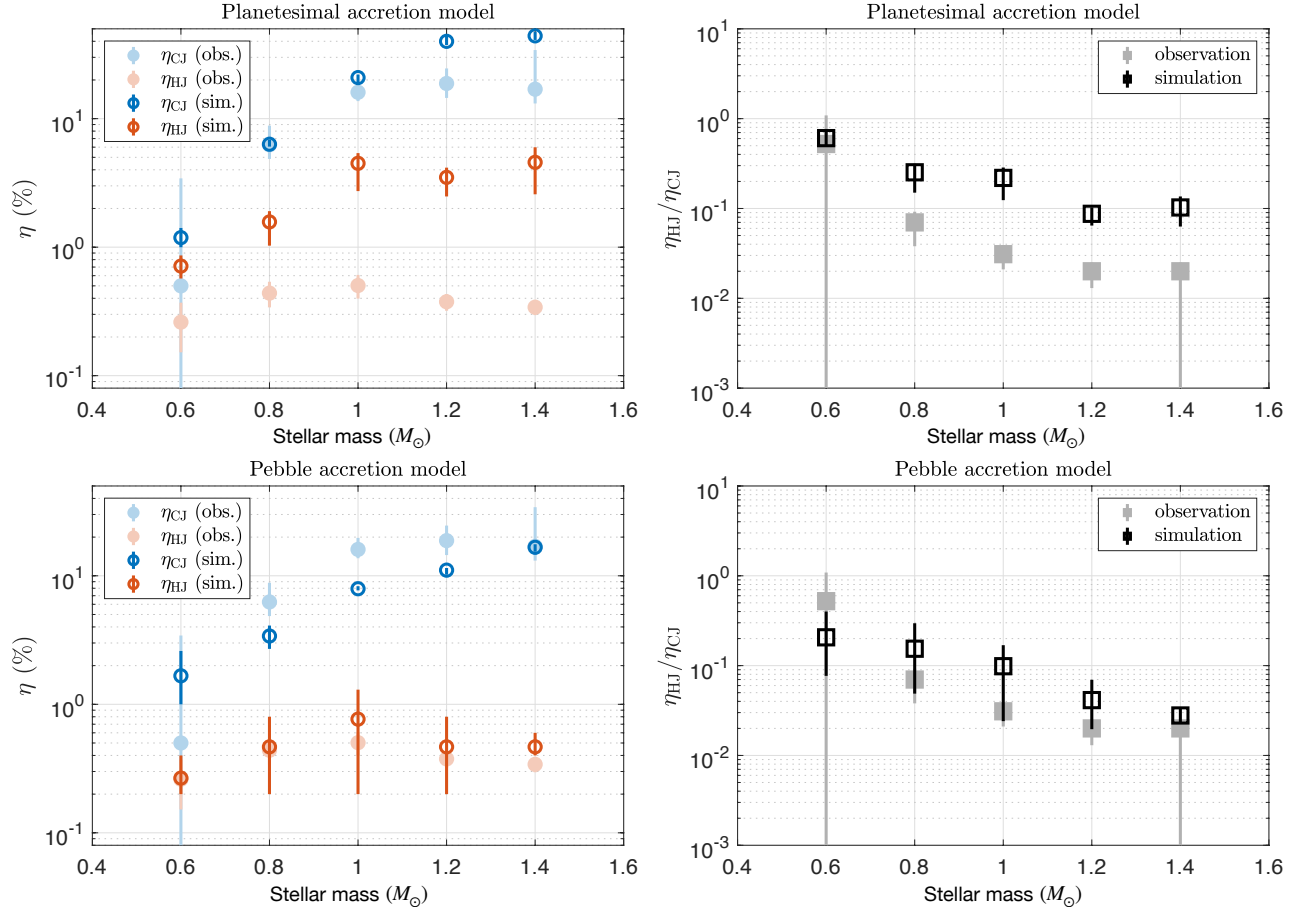


Figure 4. *Left Panels:* Simulated occurrence rate of hot Jupiters (η_{HJ}) and cold Jupiters (η_{CJ}) as a function of stellar mass. *Right Panel:* Relative occurrence rate ε between HJs and CJs ($\varepsilon = \eta_{\text{HJ}}/\eta_{\text{CJ}}$) vs. stellar mass. The top and bottom panels show results from the planetesimal and pebble accretion models. The markers show the mean values, and the error bars show the scatter of the results from three sets of simulations. The filled markers represent data from observations as in Fig. 2, and the open markers represent the simulation results.

First, we test whether the planetesimal accretion model can explain the observed correlation between ε and M_* by performing planet population synthesis simulations using the Ida & Lin model. The model details are presented in Ida et al. (2013) and Ida et al. (2018). The stellar mass has a range of 0.5 to 1.5 M_\odot and is evenly divided into 5 bins, each with a bin width of 0.2 M_\odot . Three sets of simulations are performed for each stellar mass bin. In each bin, the stellar mass is given by a normal distribution with a mean value being the bin center and a dispersion of 0.1 M_\odot . The retardation factor for orbital migration is $C_1 = 0.05$, which means that the migration speed is reduced by a factor of 20. The initial solid and gas surface density resembles the minimum mass solar nebula (MMSN, Hayashi 1981), with a scaling factor f to control the total disk mass. The total mass of the protoplanetary disk increases with the stellar mass as $f \propto M_*^{1.5}$. The planetesimal disk size

ranges from 0.5 to 20 au. Following Ida et al. (2018), we set the mass of planetesimals and the initial mass of planet embryos to be 10^{20} g. The embryos are initially distributed with orbital separations of 10 times the Hill radius of their isolation mass ($r_{\text{H}} = (m_{\text{iso}}/3M_*)^{1/3}a$). The mass accretion rates of the embryos are calculated based on the local disk surface density. For more detailed descriptions of the disk model and their methods, we refer to Ida et al. (2013) and Ida et al. (2018).

We also study the pebble accretion planet population synthesis model by conducting three sets of simulations, each of which contains 2,000 systems with Monte Carlo sampling of their initial disk and stellar properties. We only consider the growth and migration of a single protoplanet within individual systems. We assume that pebbles have all grown up to a Stokes number of 0.01, roughly equivalent to a millimeter in size. The embryo with $M_{\text{p}} = 0.01 M_\oplus$ is placed logarithmically between

0.1 and 40 au. Detailed model prescription can be found in Liu et al. (2019). One notable aspect differed from Liu et al. (2019) is that the type I migration of the planets is adopted from D’Angelo & Lubow (2010)’s 3D isothermal formula with a retardation factor of $C_1=0.1$. Other initial conditions and distributions of model parameters in the above two models are summarized in Table 3.

Figure 3 illustrates the simulated η_{HJ} , η_{CJ} and their ratio as a function of M_\star . Both models predict that η_{HJ} and η_{CJ} increase with M_\star . The increasing trend of η_{CJ} is steeper than that of η_{HJ} , while η_{HJ} mildly peaks at solar-mass stars. Consequently, the relative occurrence rate decreases with stellar mass, ranging from 0.1–1 around stars of $0.6 M_\odot$ to 0.02–0.1 around stars of $1.4 M_\odot$. These results align well with the observations shown in Figure 2. Physically, this implies that a larger fraction of giant planets form around more massive stars, but a small fraction of them undergo disk migration and transition into HJs. We note that in both models, one parameter that particularly required tuning in order to match the results with observations is the migration reduction factor C_1 . With larger values of C_1 , the simulations typically produce a higher fraction of HJs compared with observation due to efficient inward migration.

4. DISCUSSIONS AND CONCLUSIONS

In this paper we present a key indicator, the relative occurrence rate between hot and cold Jupiters ($\varepsilon = \eta_{\text{HJ}}/\eta_{\text{CJ}}$), to trace the formation and evolution of giant planet systems. Combining the statistics based on *TESS* and CLS surveys, we identify a tentative decreasing trend of ε with increasing stellar mass (97% confidence). We find that this trend could be explained by different planet growth and migration time scales around different stars through state-of-the-art planetesimal and pebble accretion simulations. Both simulations quantitatively reproduce the observed correlation between stellar mass and η_{HJ} , η_{CJ} as well as $\eta_{\text{HJ}}/\eta_{\text{CJ}}$.

4.1. Caveats

There are several caveats that we do not account for including (1) comparing occurrence rates from two techniques; (2) the statistical methodologies used in three works that this work is based on are different; (3) theoretical models that simplify the retention or destruction of planets near the inner edge of the disk.

A major caveat of this work is that we are comparing η_{CJ} from RVs and η_{HJ} from transit surveys, and η_{HJ} is known to differ by a factor of about two between these two methods. Ideally, one should use η_{CJ} and η_{HJ} estimates from the same method, but limitations

from occurrence rate studies to date prohibit such an attempt. Typical RV studies have a limited sample in HJ detections and thus do not report η_{HJ} across stellar types (Wright et al. 2012; Fulton et al. 2021), and transit surveys typically do not have the long baseline to recover a large enough sample of CJs (Hsu et al. 2019). Worse still, transiting cold Jupiters around M dwarfs have never been detected, making η_{CJ} at M dwarfs not available via transits.

To match the η_{HJ} from RVs, in principle, one could apply a correction factor to the η_{HJ} estimates from transits. The difference between η_{HJ} from RV and transits arises from the metallicity (Wright et al. 2012), binary fraction (Moe & Kratter 2021), age (Chen et al. 2023) distributions of stellar samples, or, most likely, a combination of three factors. Chen et al. (2023) found that the discrepancy of η_{HJ} between transit and RV surveys could be explained after accounting for the metallicity and age effect (and thus much less from the binarity effect). Such an effect is not yet seen to vary widely across stellar types (Miyazaki & Masuda 2023), hence it may lead to a similar occurrence rate shift at different stellar masses if we calibrate η_{HJ} from transit to RV studies, which will not significantly change the decreasing trend of ε . Although photometric surveys like *Kepler* and *TESS* have large homogeneously selected stellar samples, the stellar catalog of long-term RV surveys might be biased due to human factors and multiple selection criterias, which will lead to risks on further statistics. However, the CLS program selected targets in a statistical sense like a blind survey as California Planet Search (CPS; Howard et al. 2010) without bias toward stars more likely to host planets according to metallicity information or previous data (see Section 2 in Rosenthal et al. 2021), making such a situation less serious.

Secondly, the methodologies used in Fulton et al. (2021), Beleznav & Kunimoto (2022) and Bryant et al. (2023) to derive giant planet occurrence rates are different. Beleznav & Kunimoto (2022) utilize a Beta distribution model as in Zhou et al. (2019), where the number of observed planets is computed with a false positive rate according to the dispositions of planet candidates and a weighting parameter of the probability that a star falls in a specific mass bin. The effective number of stars is determined based on the detection sensitivity and completeness through injection and recovery tests. The statistical method applied in Bryant et al. (2023) is similar to Beleznav & Kunimoto (2022) but estimating false positive rate through a Bayesian way instead, and without taking the aforementioned weighting parameter into consideration. In terms of cold Jupiters, Fulton et al. (2021) employed the hierarchical Bayesian methodology

Table 3. Model parameters in population synthesis models.

Parameters (Planetesimal model)	Value	Description
$\alpha_{\text{vis}}, \alpha_{\text{acc}}$	$3 \times 10^{-4}, 3 \times 10^{-3}$	Disk α viscosity (turbulent, accretion).
k_1, k_2	9, 3.5	Gas contraction ^[1] .
[Fe/H]	$\mathcal{N}^{[2]}(\mu, \sigma^2), \mu = 0, \sigma = 0.2$	Metallicity.
$\log(\tau_{\text{disk}} [\text{yr}])$	$\mathcal{N}(\mu, \sigma^2), \mu = 6.5, \sigma = 0.2$	Disk lifetime.
$\log(f)$	$\mathcal{N}(\mu, \sigma^2), \mu = 0, \sigma = 0.1$	Disk mass scaling factor.
p_{disk}	1.5	$f \propto M_{\star}^{p_{\text{disk}}}$.
C_1	0.05	Migration retardation factor.

Parameters (Pebble model)	Value	Description
$\dot{M}_{\text{g0}} (M_{\odot} \text{ yr}^{-1})$	$10^{\mathcal{N}(\mu, \sigma^2)} \times (M_{\star}/M_{\odot})^{1.5}, \mu = -7.5, \sigma = 0.3$	Disk accretion rate.
$R_{\text{d0}} (\text{AU})$	$\mathcal{U}^{[3]}(50, 200) \times (M_{\star}/M_{\odot})$	Disk size.
[Fe/H]	$\mathcal{N}(\mu, \sigma^2), \mu = -0.03, \sigma = 0.2$	Metallicity.
ξ	$0.0149 \times 10^{\mathcal{N}(\mu, \sigma^2)}, \mu = -0.03, \sigma = 0.2$	Pebble-to-gas flux ratio.
α_{g}	10^{-2}	Global viscous coefficient.
α_{t}	10^{-3}	Midplane turbulent strength.
τ_{s}	10^{-2}	Pebbles' Stokes number.
C_1	0.1	Migration retardation factor.

[1] The gas contraction timescale is $\tau_{\text{KH}} \simeq 10^{k_1} (M_{\text{p}}/M_{\oplus})^{-k_2}$ yr.

[2] $\mathcal{N}(\mu, \sigma^2)$ means a normal distribution with mean μ and standard deviation σ .

[3] $\mathcal{U}(a, b)$ stands for a uniform distribution between a and b .

described in [Hogg et al. \(2010\)](#) and [Foreman-Mackey et al. \(2014\)](#), which is different from the other two works. We note that we do not adjust these difference in this work and we assume the final occurrence rate outputs (N_p per 100 stars) are not biased between statistical methodologies.

From the simulation side, we only test if the trend can be explained by a single formation mechanism of CJ and HJs: via core accretion plus disk migration. High-eccentricity migration and disk instability are also expected to affect the formation of HJ and CJ systems ([Dawson & Johnson 2018](#)). Theoretical simulations under these frameworks to examine whether they could reproduce the decreasing trend of ε might be a way to figure out if they played a dominant role compared with disk migration. A major limitation of our simulation is that the models employed are simplified in the sense of describing the evolution of planets after migrating to the inner edge of the protoplanetary disk, because other than the balance between growth and migration as the stellar mass changes, the dependence of the retention efficiency of HJs by the inner disk cavity on the stellar mass may also contribute to the observed decreasing trend of ε . For simplicity, the Ida & Lin model assumes a fixed location for the inner disk edge that does not depend on the central body mass. In the pebble accretion model, a static inner disk edge is assumed to approximate to the co-rotation radius of the central

star. In both models, the inner edge of the disk serves as the location to halt the inward migration of planets. In principle, the inner cavity radius is determined by a balance between the stellar magnetic torque and the gas accretion torque ([Koenigl 1991](#); [Lin et al. 1996](#); [Liu et al. 2017](#)). For massive stars ($\gtrsim 1.5 M_{\odot}$), the magnetic fields can be too weak to clear up a magnetospheric cavity in the inner disk due to the lack of convective zones, making it difficult to halt the inward migration of HJs. In this regard, giant planets are more easily trapped at the inner disk edge around low-mass dwarfs, while they are more likely to migrate inward and eventually collide with the central stars in systems around more massive stars. In addition, several other mechanisms that could potentially destroy these close-in planets, such as the tidal interaction and disruption ([Liu et al. 2013](#)) or engulfment of planets ([De et al. 2023](#)) by the central star, have not been considered in both models.

4.2. Relative Occurrence Rate Results from Kepler

The *Kepler* mission has produced lots of occurrence rate results for giant planets around FGK stars ([Fressin et al. 2013](#); [Howard et al. 2012](#); [Petigura et al. 2018](#); [Hsu et al. 2019](#); [Kunimoto & Matthews 2020](#)). The completeness as well as reliability of occurrence rates are also well-studied ([Burke et al. 2015](#); [Bryson et al. 2020](#)). Therefore, it is worth looking into these results

in a similar way and revisiting the trend between the relative occurrence rate ε and stellar mass M_\star .

As a reference, we retrieve the results of η from [Kunimoto & Matthews \(2020\)](#), who presented the planet occurrence rates over the period–radius grid recommended by the Study Analysis Group (SAG) 13 of the NASA Exoplanet Exploration Program Analysis Group (ExoPAG). The whole stellar sample was divided into three categories based on the suggested T_{eff} limits from [Pecaut & Mamajek \(2013\)](#): F- ($6000 \leq T_{\text{eff}} \leq 7300$ K), G- ($5300 \leq T_{\text{eff}} \leq 6000$ K) and K-type ($3900 \leq T_{\text{eff}} \leq 5300$ K) stars, different with the selection according to stellar mass used in this work. For the giant planet group, there are η measurements in two radius ($7.59\text{--}11.39$ and $11.39\text{--}17.09 R_\oplus$) and six period ($10\text{--}20$, $20\text{--}40$, $40\text{--}80$, $80\text{--}160$, $160\text{--}320$, $320\text{--}640$ days) bins (see Figure 5).

The uncertainties of η are higher compared with the results from *TESS* listed in Table 2, which will consequently lead to higher uncertainties on ε if compared with the RV result from CLS. In principle, one can homogeneously measure ε based on the existing *Kepler* occurrence rate results from the literature, though within two semi-major axis ranges close to the host star. However, we note that the differences of the semi-major axis boundary of three stellar types will be more significant (~ 0.4 AU) towards large period bins when performing the conversion. With these in mind, we compute the ε based on η from the first period bin and others, attempting to investigate the relation between ε and T_{eff} . The results are presented in Figure 6. Due to the large uncertainty of ε , we are not able to claim any trend.

4.3. Future Prospects

At present, the confidence level of the decreasing trend between ε and stellar mass M_\star is not high. Future observations are required to revisit this parameter, and confirm or rule out the anti-correlation. Here, we suggest two possible ways to improve the significance of the trend.

Due to the limited sample size of CJs around M dwarfs, the constraint on their occurrence rate still has a large uncertainty, especially if attempting to group them into different stellar mass and semi-major axis bins. Including additional η_{CJ} data points of M dwarfs with stellar mass below $0.65 M_\odot$, in particular mid-to-late M stars, would make the behaviour of ε more clear. However, we emphasize that such measurements should be done under the same definition of CJs ($100 M_\oplus \leq M_p \leq 13.6 M_J$, $1 \leq a \leq 5$ au) otherwise they cannot be directly compared with the results in this work. Ground-based blind RV surveys, notably in the near-infrared band, definitely provide a pathway to constrain

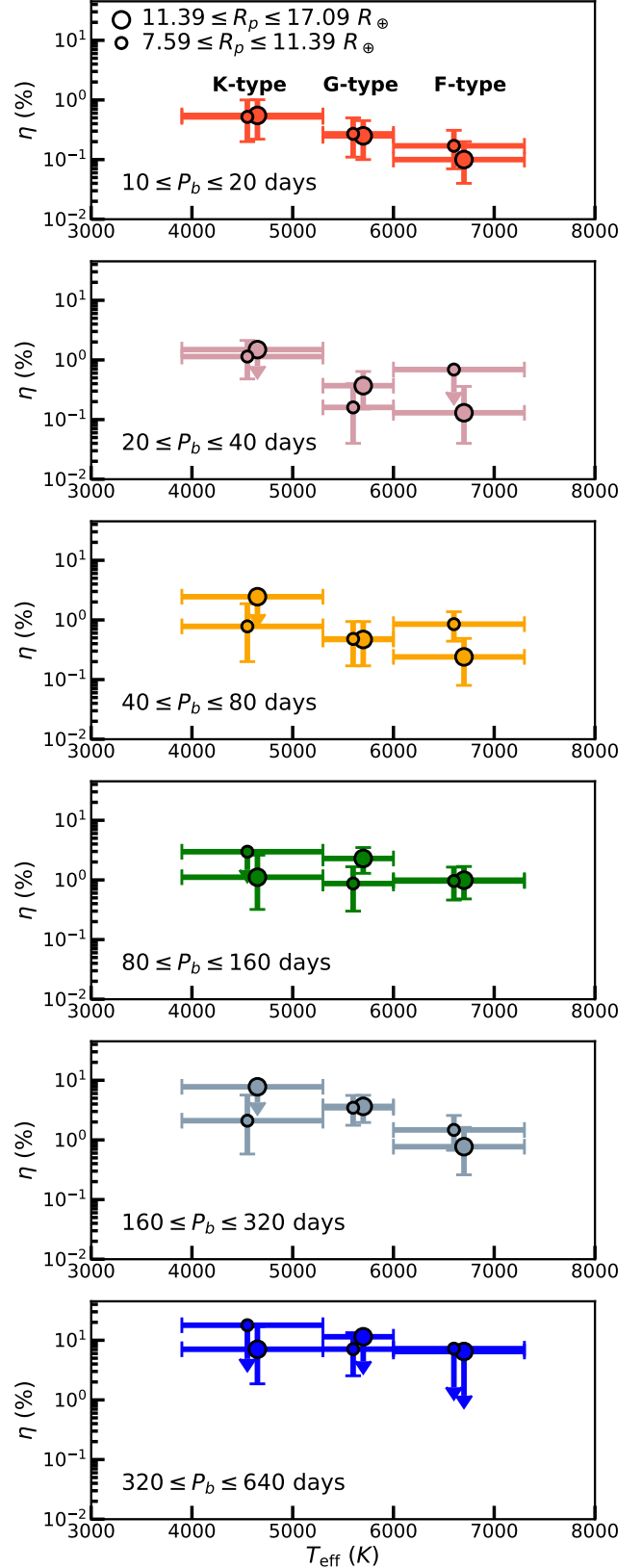


Figure 5. Giant planet occurrence rate vs. stellar effective temperature based on *Kepler* mission taken from [Kunimoto & Matthews \(2020\)](#). Different panels show results of different period bins. The marker size scales with planet radius ranges shown on the top left in the first panel. We add small shifts to the horizontal coordinates for clarity.

the η_{CJ} around M dwarfs (e.g., Morales et al. 2019; Stefansson et al. 2023). Microlensing (Mao & Paczynski 1991; Gould & Loeb 1992) and direct imaging (Montet et al. 2014; Zhang et al. 2021) have also shown their capability in discovering cold giants around M stars, though the detection rates of these two techniques are relatively low.

Astrometry is a promising route to efficiently find long-period planets in the near future. Based on the absolute astrometry measurements from *Hipparcos* (Perryman et al. 1997; van Leeuwen 2007) and *Gaia* (Gaia Collaboration et al. 2018, 2021) as well as ground RVs, a considerable number of CJs have been confirmed with true mass obtained (e.g., Feng et al. 2022; Sozzetti 2023). With the astrometry method, we are able to determine η_{CJ} across stars with a wide range of mass, providing a check independent of RV (Perryman et al. 2014). The astronomic signal is proportional to the mass ratio of the planetary system, making it sensitive to giant planets around low-mass stars. Moreover, the detections of planets around more massive stars, for example A-type stars (e.g., Collier Cameron et al. 2010; Gaudi et al. 2017; Zhou et al. 2019), are limited by their shallow transit depth and small RV amplitude. Such constraints are slightly mitigated when tracking the stellar motions. Extending the ε function to A and F stars with mass between 1.4 and 2.0 M_{\odot} will enable the exploration toward the high-mass end. Although the *Gaia* DR4 time-series astrometric data would not be available before the end of 2025, the non-single-star catalog with two body or-

bit solutions released during DR3 (Gaia Collaboration et al. 2023; Halbwachs et al. 2023; Holl et al. 2023) have already enabled the true mass determination for several CJs (Winn 2022; Gan 2023).

Finally, we suggest using similar definitions of both HJs and CJs in future demographic works, which will enable joint analysis across different parameter space, making the comparisons between different results easier.

5. ACKNOWLEDGMENTS

We thank Doug Lin, Shigeru Ida and Yasunori Hori for useful discussions, and two anonymous referees for their comments that improved the quality of this paper.

This work is supported by the National Science Foundation of China (Grant No. 12133005). K. Guo acknowledges the access to Matlab R2021b under the academic license granted by Shanghai Jiao Tong University. BL acknowledges the fundings from the National Natural Science Foundation of China (Nos. 12222303, 12173035, 12147103 and 12111530175), the start-up grant of the Bairen program from Zhejiang University and the Fundamental Research Funds for the Central Universities (2022-KYY-506107-0001,226-2022-00216).

Facilities: TESS, Kepler, Keck

Software: numpy (van der Walt et al. 2011), matplotlib (Hunter 2007), scipy (Virtanen et al. 2020)

APPENDIX

A. RELATIVE OCCURRENCE RATE RESULTS FROM *Kepler* MISSION

We compute the relative occurrence rate ε based on *Kepler*-only results from Kunimoto & Matthews (2020). We note that the calculations are done in the period bins instead of semi-major axis bins.

REFERENCES

- Akeson, R. L., Chen, X., Ciardi, D., et al. 2013, *PASP*, 125, 989, doi: [10.1086/672273](https://doi.org/10.1086/672273)
- Andrews, S. M., Rosenfeld, K. A., Kraus, A. L., & Wilner, D. J. 2013, *ApJ*, 771, 129, doi: [10.1088/0004-637X/771/2/129](https://doi.org/10.1088/0004-637X/771/2/129)
- Baglin, A., Auvergne, M., Barge, P., et al. 2006, in *ESA Special Publication, Vol. 1306, The CoRoT Mission Pre-Launch Status - Stellar Seismology and Planet Finding*, ed. M. Fridlund, A. Baglin, J. Lochard, & L. Conroy, 33
- Bakos, G., Noyes, R. W., Kovács, G., et al. 2004, *PASP*, 116, 266, doi: [10.1086/382735](https://doi.org/10.1086/382735)
- Beleznay, M., & Kunimoto, M. 2022, *MNRAS*, 516, 75, doi: [10.1093/mnras/stac2179](https://doi.org/10.1093/mnras/stac2179)
- Borucki, W. J., Koch, D., Basri, G., et al. 2010, *Science*, 327, 977, doi: [10.1126/science.1185402](https://doi.org/10.1126/science.1185402)
- Boss, A. P. 1997, *Science*, 276, 1836, doi: [10.1126/science.276.5320.1836](https://doi.org/10.1126/science.276.5320.1836)
- Bryant, E. M., Bayliss, D., & Van Eylen, V. 2023, *MNRAS*, doi: [10.1093/mnras/stad626](https://doi.org/10.1093/mnras/stad626)

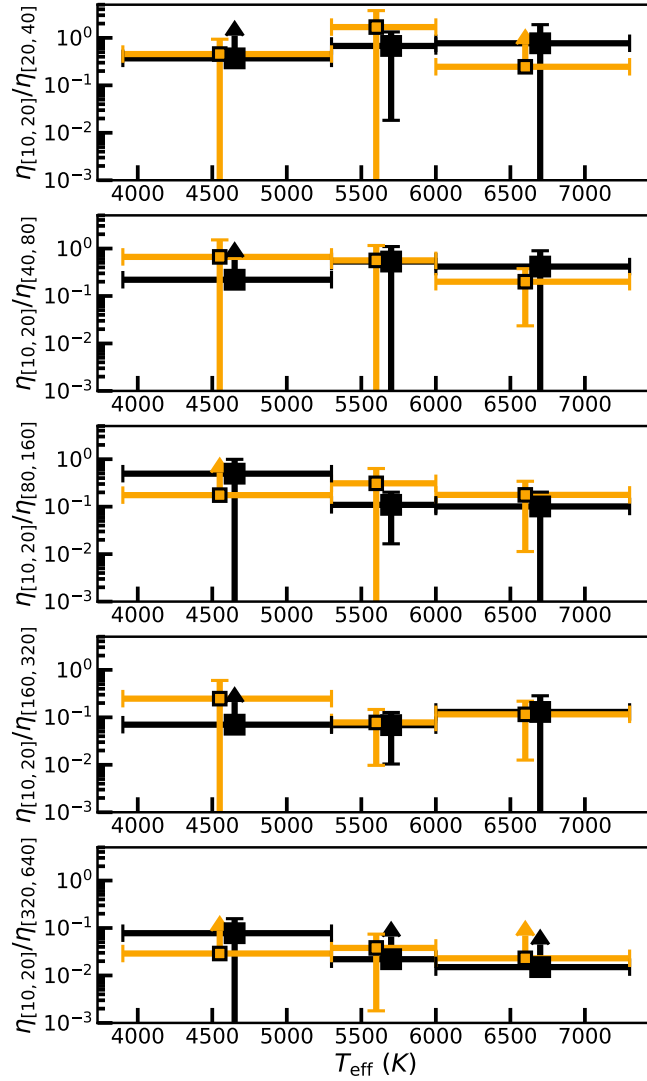


Figure 6. Relative occurrence rate based on the occurrence rate results from [Kunimoto & Matthews \(2020\)](#) as a function of effective temperature. The small orange and large black squares are the results of giant planets within two different radius ranges, $7.59 \leq R_p \leq 11.39 R_{\oplus}$ and $11.39 \leq R_p \leq 17.09 R_{\oplus}$ (see Figure 5 and Section 4.2 for details). The subscripts of η represent the period bins. We add small shifts to the horizontal coordinates for clarity.

Bryson, S. 2020, *Research Notes of the American Astronomical Society*, 4, 32,
doi: [10.3847/2515-5172/ab7afd](https://doi.org/10.3847/2515-5172/ab7afd)

Bryson, S., Coughlin, J., Batalha, N. M., et al. 2020, *AJ*, 159, 279, doi: [10.3847/1538-3881/ab8a30](https://doi.org/10.3847/1538-3881/ab8a30)

Burke, C. J., Christiansen, J. L., Mullally, F., et al. 2015, *ApJ*, 809, 8, doi: [10.1088/0004-637X/809/1/8](https://doi.org/10.1088/0004-637X/809/1/8)

Burkert, A., & Ida, S. 2007, *ApJ*, 660, 845,
doi: [10.1086/512538](https://doi.org/10.1086/512538)

Burn, R., Schlecker, M., Mordasini, C., et al. 2021, *A&A*, 656, A72, doi: [10.1051/0004-6361/202140390](https://doi.org/10.1051/0004-6361/202140390)

Chazelas, B., Pollacco, D., Queloz, D., et al. 2012, in *Society of Photo-Optical Instrumentation Engineers (SPIE) Conference Series*, Vol. 8444, *Ground-based and Airborne Telescopes IV*, 84440E, doi: [10.1117/12.925755](https://doi.org/10.1117/12.925755)

Chen, D.-C., Xie, J.-W., Zhou, J.-L., et al. 2023, *Proceedings of the National Academy of Science*, 120, e2304179120, doi: [10.1073/pnas.2304179120](https://doi.org/10.1073/pnas.2304179120)

Collier Cameron, A., Guenther, E., Smalley, B., et al. 2010, *MNRAS*, 407, 507, doi: [10.1111/j.1365-2966.2010.16922.x](https://doi.org/10.1111/j.1365-2966.2010.16922.x)

Cumming, A., Butler, R. P., Marcy, G. W., et al. 2008, *PASP*, 120, 531, doi: [10.1086/588487](https://doi.org/10.1086/588487)

D'Angelo, G., & Lubow, S. H. 2010, *ApJ*, 724, 730,
doi: [10.1088/0004-637X/724/1/730](https://doi.org/10.1088/0004-637X/724/1/730)

- Dawson, R. I., & Johnson, J. A. 2018, *ARA&A*, 56, 175, doi: [10.1146/annurev-astro-081817-051853](https://doi.org/10.1146/annurev-astro-081817-051853)
- De, K., MacLeod, M., Karambelkar, V., et al. 2023, *Nature*, 617, 55, doi: [10.1038/s41586-023-05842-x](https://doi.org/10.1038/s41586-023-05842-x)
- Dressing, C. D., & Charbonneau, D. 2013, *ApJ*, 767, 95, doi: [10.1088/0004-637X/767/1/95](https://doi.org/10.1088/0004-637X/767/1/95)
- . 2015, *ApJ*, 807, 45, doi: [10.1088/0004-637X/807/1/45](https://doi.org/10.1088/0004-637X/807/1/45)
- Drażkowska, J., Bitsch, B., Lambrechts, M., et al. 2023, in *Astronomical Society of the Pacific Conference Series*, Vol. 534, *Protostars and Planets VII*, ed. S. Inutsuka, Y. Aikawa, T. Muto, K. Tomida, & M. Tamura, 717, doi: [10.48550/arXiv.2203.09759](https://doi.org/10.48550/arXiv.2203.09759)
- Endl, M., Cochran, W. D., Kürster, M., et al. 2006, *ApJ*, 649, 436, doi: [10.1086/506465](https://doi.org/10.1086/506465)
- Feng, F., Butler, R. P., Vogt, S. S., et al. 2022, *ApJS*, 262, 21, doi: [10.3847/1538-4365/ac7e57](https://doi.org/10.3847/1538-4365/ac7e57)
- Foreman-Mackey, D., Hogg, D. W., & Morton, T. D. 2014, *ApJ*, 795, 64, doi: [10.1088/0004-637X/795/1/64](https://doi.org/10.1088/0004-637X/795/1/64)
- Fressin, F., Torres, G., Charbonneau, D., et al. 2013, *ApJ*, 766, 81, doi: [10.1088/0004-637X/766/2/81](https://doi.org/10.1088/0004-637X/766/2/81)
- Fulton, B. J., Rosenthal, L. J., Hirsch, L. A., et al. 2021, *ApJS*, 255, 14, doi: [10.3847/1538-4365/abfcc1](https://doi.org/10.3847/1538-4365/abfcc1)
- Gaia Collaboration, Brown, A. G. A., Vallenari, A., et al. 2018, *A&A*, 616, A1, doi: [10.1051/0004-6361/201833051](https://doi.org/10.1051/0004-6361/201833051)
- . 2021, *A&A*, 649, A1, doi: [10.1051/0004-6361/202039657](https://doi.org/10.1051/0004-6361/202039657)
- Gaia Collaboration, Vallenari, A., Brown, A. G. A., et al. 2023, *A&A*, 674, A1, doi: [10.1051/0004-6361/202243940](https://doi.org/10.1051/0004-6361/202243940)
- Gaidos, E., Mann, A. W., Kraus, A. L., & Ireland, M. 2016, *MNRAS*, 457, 2877, doi: [10.1093/mnras/stw097](https://doi.org/10.1093/mnras/stw097)
- Gan, T. 2023, *Research Notes of the American Astronomical Society*, 7, 226, doi: [10.3847/2515-5172/ad0643](https://doi.org/10.3847/2515-5172/ad0643)
- Gan, T., Wang, S. X., Wang, S., et al. 2023, *AJ*, 165, 17, doi: [10.3847/1538-3881/ac9b12](https://doi.org/10.3847/1538-3881/ac9b12)
- Gaudi, B. S., Stassun, K. G., Collins, K. A., et al. 2017, *Nature*, 546, 514, doi: [10.1038/nature22392](https://doi.org/10.1038/nature22392)
- Gould, A., Dorsher, S., Gaudi, B. S., & Udalski, A. 2006, *AcA*, 56, 1. <https://arxiv.org/abs/astro-ph/0601001>
- Gould, A., & Loeb, A. 1992, *ApJ*, 396, 104, doi: [10.1086/171700](https://doi.org/10.1086/171700)
- Guo, K., & Kokubo, E. 2021, *AJ*, 162, 115, doi: [10.3847/1538-3881/ac0895](https://doi.org/10.3847/1538-3881/ac0895)
- Halbwachs, J.-L., Pourbaix, D., Arenou, F., et al. 2023, *A&A*, 674, A9, doi: [10.1051/0004-6361/202243969](https://doi.org/10.1051/0004-6361/202243969)
- Hardegree-Ullman, K. K., Cushing, M. C., Muirhead, P. S., & Christiansen, J. L. 2019, *AJ*, 158, 75, doi: [10.3847/1538-3881/ab21d2](https://doi.org/10.3847/1538-3881/ab21d2)
- Hartmann, L., Herczeg, G., & Calvet, N. 2016, *ARA&A*, 54, 135, doi: [10.1146/annurev-astro-081915-023347](https://doi.org/10.1146/annurev-astro-081915-023347)
- Hayashi, C. 1981, *Progress of Theoretical Physics Supplement*, 70, 35, doi: [10.1143/PTPS.70.35](https://doi.org/10.1143/PTPS.70.35)
- Hogg, D. W., Myers, A. D., & Bovy, J. 2010, *ApJ*, 725, 2166, doi: [10.1088/0004-637X/725/2/2166](https://doi.org/10.1088/0004-637X/725/2/2166)
- Holl, B., Sozzetti, A., Sahlmann, J., et al. 2023, *A&A*, 674, A10, doi: [10.1051/0004-6361/202244161](https://doi.org/10.1051/0004-6361/202244161)
- Howard, A. W., Johnson, J. A., Marcy, G. W., et al. 2010, *ApJ*, 721, 1467, doi: [10.1088/0004-637X/721/2/1467](https://doi.org/10.1088/0004-637X/721/2/1467)
- Howard, A. W., Marcy, G. W., Bryson, S. T., et al. 2012, *ApJS*, 201, 15, doi: [10.1088/0067-0049/201/2/15](https://doi.org/10.1088/0067-0049/201/2/15)
- Howell, S. B., Sobeck, C., Haas, M., et al. 2014, *PASP*, 126, 398, doi: [10.1086/676406](https://doi.org/10.1086/676406)
- Hsu, D. C., Ford, E. B., Ragozzine, D., & Ashby, K. 2019, *AJ*, 158, 109, doi: [10.3847/1538-3881/ab31ab](https://doi.org/10.3847/1538-3881/ab31ab)
- Hunter, J. D. 2007, *Computing in Science & Engineering*, 9, 90, doi: [10.1109/MCSE.2007.55](https://doi.org/10.1109/MCSE.2007.55)
- Ida, S., & Lin, D. N. C. 2004, *ApJ*, 604, 388, doi: [10.1086/381724](https://doi.org/10.1086/381724)
- Ida, S., Lin, D. N. C., & Nagasawa, M. 2013, *ApJ*, 775, 42, doi: [10.1088/0004-637X/775/1/42](https://doi.org/10.1088/0004-637X/775/1/42)
- Ida, S., Tanaka, H., Johansen, A., Kanagawa, K. D., & Tanigawa, T. 2018, *ApJ*, 864, 77, doi: [10.3847/1538-4357/aad69c](https://doi.org/10.3847/1538-4357/aad69c)
- Ikoma, M., Nakazawa, K., & Emori, H. 2000, *ApJ*, 537, 1013, doi: [10.1086/309050](https://doi.org/10.1086/309050)
- Johnson, J. A., Howard, A. W., Marcy, G. W., et al. 2010, *PASP*, 122, 149, doi: [10.1086/651007](https://doi.org/10.1086/651007)
- Johnson, J. A., Gazak, J. Z., Apps, K., et al. 2012, *AJ*, 143, 111, doi: [10.1088/0004-6256/143/5/111](https://doi.org/10.1088/0004-6256/143/5/111)
- Johnston, H. F., Panić, O., & Liu, B. 2023, *MNRAS*, doi: [10.1093/mnras/stad3254](https://doi.org/10.1093/mnras/stad3254)
- Koenigl, A. 1991, *ApJL*, 370, L39, doi: [10.1086/185972](https://doi.org/10.1086/185972)
- Kovács, G., Hodgkin, S., Sipőcz, B., et al. 2013, *MNRAS*, 433, 889, doi: [10.1093/mnras/stt571](https://doi.org/10.1093/mnras/stt571)
- Kunimoto, M., & Matthews, J. M. 2020, *AJ*, 159, 248, doi: [10.3847/1538-3881/ab88b0](https://doi.org/10.3847/1538-3881/ab88b0)
- Lin, D. N. C., Bodenheimer, P., & Richardson, D. C. 1996, *Nature*, 380, 606, doi: [10.1038/380606a0](https://doi.org/10.1038/380606a0)
- Liu, B., & Ji, J. 2020, *Research in Astronomy and Astrophysics*, 20, 164, doi: [10.1088/1674-4527/20/10/164](https://doi.org/10.1088/1674-4527/20/10/164)
- Liu, B., Lambrechts, M., Johansen, A., & Liu, F. 2019, *A&A*, 632, A7, doi: [10.1051/0004-6361/201936309](https://doi.org/10.1051/0004-6361/201936309)
- Liu, B., & Ormel, C. W. 2018, *A&A*, 615, A138, doi: [10.1051/0004-6361/201732307](https://doi.org/10.1051/0004-6361/201732307)
- Liu, B., Ormel, C. W., & Lin, D. N. C. 2017, *A&A*, 601, A15, doi: [10.1051/0004-6361/201630017](https://doi.org/10.1051/0004-6361/201630017)
- Liu, S.-F., Guillochon, J., Lin, D. N. C., & Ramirez-Ruiz, E. 2013, *ApJ*, 762, 37, doi: [10.1088/0004-637X/762/1/37](https://doi.org/10.1088/0004-637X/762/1/37)
- Mao, S., & Paczynski, B. 1991, *ApJL*, 374, L37, doi: [10.1086/186066](https://doi.org/10.1086/186066)

- Mayor, M., & Queloz, D. 1995, *Nature*, 378, 355, doi: [10.1038/378355a0](https://doi.org/10.1038/378355a0)
- Mayor, M., Marmier, M., Lovis, C., et al. 2011, arXiv e-prints, arXiv:1109.2497, <https://arxiv.org/abs/1109.2497>
- Miyazaki, S., & Masuda, K. 2023, *AJ*, 166, 209, doi: [10.3847/1538-3881/acff71](https://doi.org/10.3847/1538-3881/acff71)
- Moe, M., & Kratter, K. M. 2021, *MNRAS*, 507, 3593, doi: [10.1093/mnras/stab2328](https://doi.org/10.1093/mnras/stab2328)
- Montet, B. T., Crepp, J. R., Johnson, J. A., Howard, A. W., & Marcy, G. W. 2014, *ApJ*, 781, 28, doi: [10.1088/0004-637X/781/1/28](https://doi.org/10.1088/0004-637X/781/1/28)
- Morales, J. C., Mustill, A. J., Ribas, I., et al. 2019, *Science*, 365, 1441, doi: [10.1126/science.aax3198](https://doi.org/10.1126/science.aax3198)
- Mordasini, C., Alibert, Y., & Benz, W. 2009, *A&A*, 501, 1139, doi: [10.1051/0004-6361/200810301](https://doi.org/10.1051/0004-6361/200810301)
- Morton, T. D., & Swift, J. 2014, *ApJ*, 791, 10, doi: [10.1088/0004-637X/791/1/10](https://doi.org/10.1088/0004-637X/791/1/10)
- Muirhead, P. S., Mann, A. W., Vanderburg, A., et al. 2015, *ApJ*, 801, 18, doi: [10.1088/0004-637X/801/1/18](https://doi.org/10.1088/0004-637X/801/1/18)
- Mulders, G. D., Pascucci, I., & Apai, D. 2015, *ApJ*, 798, 112, doi: [10.1088/0004-637X/798/2/112](https://doi.org/10.1088/0004-637X/798/2/112)
- Pan, M., Liu, B., Johansen, A., et al. 2024, *A&A*, 682, A89, doi: [10.1051/0004-6361/202347664](https://doi.org/10.1051/0004-6361/202347664)
- Pecaut, M. J., & Mamajek, E. E. 2013, *ApJS*, 208, 9, doi: [10.1088/0067-0049/208/1/9](https://doi.org/10.1088/0067-0049/208/1/9)
- Pepper, J., Pogge, R. W., DePoy, D. L., et al. 2007, *PASP*, 119, 923, doi: [10.1086/521836](https://doi.org/10.1086/521836)
- Perryman, M., Hartman, J., Bakos, G. Á., & Lindegren, L. 2014, *ApJ*, 797, 14, doi: [10.1088/0004-637X/797/1/14](https://doi.org/10.1088/0004-637X/797/1/14)
- Perryman, M. A. C., Lindegren, L., Kovalevsky, J., et al. 1997, *A&A*, 323, L49
- Petigura, E. A., Marcy, G. W., Winn, J. N., et al. 2018, *AJ*, 155, 89, doi: [10.3847/1538-3881/aaa54c](https://doi.org/10.3847/1538-3881/aaa54c)
- Pollacco, D. L., Skillen, I., Collier Cameron, A., et al. 2006, *PASP*, 118, 1407, doi: [10.1086/508556](https://doi.org/10.1086/508556)
- Pollack, J. B., Hubickyj, O., Bodenheimer, P., et al. 1996, *Icarus*, 124, 62, doi: [10.1006/icar.1996.0190](https://doi.org/10.1006/icar.1996.0190)
- Reffert, S., Bergmann, C., Quirrenbach, A., Trifonov, T., & Künstler, A. 2015, *A&A*, 574, A116, doi: [10.1051/0004-6361/201322360](https://doi.org/10.1051/0004-6361/201322360)
- Ribas, Á., Bouy, H., & Merín, B. 2015, *A&A*, 576, A52, doi: [10.1051/0004-6361/201424846](https://doi.org/10.1051/0004-6361/201424846)
- Ricker, G. R., Winn, J. N., Vanderspek, R., et al. 2015, *Journal of Astronomical Telescopes, Instruments, and Systems*, 1, 014003, doi: [10.1117/1.JATIS.1.1.014003](https://doi.org/10.1117/1.JATIS.1.1.014003)
- Rosenthal, L. J., Fulton, B. J., Hirsch, L. A., et al. 2021, *ApJS*, 255, 8, doi: [10.3847/1538-4365/abe23c](https://doi.org/10.3847/1538-4365/abe23c)
- Sabotta, S., Schlecker, M., Chaturvedi, P., et al. 2021, *A&A*, 653, A114, doi: [10.1051/0004-6361/202140968](https://doi.org/10.1051/0004-6361/202140968)
- Schoonenberg, D., Liu, B., Ormel, C. W., & Dorn, C. 2019, *A&A*, 627, A149, doi: [10.1051/0004-6361/201935607](https://doi.org/10.1051/0004-6361/201935607)
- Sozzetti, A. 2023, *A&A*, 670, L17, doi: [10.1051/0004-6361/202245454](https://doi.org/10.1051/0004-6361/202245454)
- Stefansson, G., Mahadevan, S., Miguel, Y., et al. 2023, arXiv e-prints, arXiv:2303.13321, doi: [10.48550/arXiv.2303.13321](https://doi.org/10.48550/arXiv.2303.13321)
- Stephan, A. P., Naoz, S., & Gaudi, B. S. 2018, *AJ*, 156, 128, doi: [10.3847/1538-3881/aad6e5](https://doi.org/10.3847/1538-3881/aad6e5)
- Su, X.-N., Zhang, H., & Zhou, J.-L. 2024, *MNRAS*, doi: [10.1093/mnras/stae733](https://doi.org/10.1093/mnras/stae733)
- van der Walt, S., Colbert, S. C., & Varoquaux, G. 2011, *Computing in Science and Engineering*, 13, 22, doi: [10.1109/MCSE.2011.37](https://doi.org/10.1109/MCSE.2011.37)
- van Leeuwen, F. 2007, *A&A*, 474, 653, doi: [10.1051/0004-6361:20078357](https://doi.org/10.1051/0004-6361:20078357)
- Virtanen, P., Gommers, R., Oliphant, T. E., et al. 2020, *Nature Methods*, 17, 261, doi: [10.1038/s41592-019-0686-2](https://doi.org/10.1038/s41592-019-0686-2)
- Winn, J. N. 2022, *AJ*, 164, 196, doi: [10.3847/1538-3881/ac9126](https://doi.org/10.3847/1538-3881/ac9126)
- Wittenmyer, R. A., Wang, S., Horner, J., et al. 2020, *MNRAS*, 492, 377, doi: [10.1093/mnras/stz3436](https://doi.org/10.1093/mnras/stz3436)
- Wolthoff, V., Reffert, S., Quirrenbach, A., et al. 2022, *A&A*, 661, A63, doi: [10.1051/0004-6361/202142501](https://doi.org/10.1051/0004-6361/202142501)
- Wright, J. T., Marcy, G. W., Howard, A. W., et al. 2012, *ApJ*, 753, 160, doi: [10.1088/0004-637X/753/2/160](https://doi.org/10.1088/0004-637X/753/2/160)
- Zhang, Z., Liu, M. C., Claytor, Z. R., et al. 2021, *ApJL*, 916, L11, doi: [10.3847/2041-8213/ac1123](https://doi.org/10.3847/2041-8213/ac1123)
- Zhou, G., Huang, C. X., Bakos, G. Á., et al. 2019, *AJ*, 158, 141, doi: [10.3847/1538-3881/ab36b5](https://doi.org/10.3847/1538-3881/ab36b5)